Weak Thermocline Mixing in the North Pacific Low-Latitude Western Boundary Current System

Zhiyu Liu[1] [ID]**, Qiang Lian[1,2], Fangtao Zhang[1], Lei Wang[1], Mingming Li[3], Xiaolin Bai[1]** [ID]**, Jianing Wang[4]** [ID] **, and Fan Wang[4]**

[1] State Key Laboratory of Marine Environmental Science, and Department of Physical Oceanography, College of Ocean and Earth Sciences, Xiamen University, Xiamen, China, [2] College of Earth, Ocean, and Atmospheric Sciences, Oregon State University, Corvallis, OR, USA, [3] College of Oceanography and Meteorology, Guangdong Ocean University, Zhanjiang, China, [4] Key Laboratory of Ocean Circulation and Waves, Institute of Oceanology, Chinese Academy of Sciences, Qingdao, China

Abstract Despite its potential importance in the global climate system, mixing properties of the North Pacific low-latitude western boundary current system (LLWBC) remained unsampled until very recently. We report here on the first measurements of turbulence microstructure associated with these currents, made in the western boundary region of the tropical North Pacific east of the Philippines. The results suggest that thermocline mixing in the North Pacific LLWBC is generally weak with the diapycnal diffusivity $\kappa_\rho \sim O(10^{-6})$ m^2 s^{-1}. This is consistent with predictions from internal wave-wave interaction theory that mixing due to internal wave breaking is significantly reduced at low latitudes. Enhanced mixing is found to be associated with a permanent cyclonic eddy, the Mindanao Eddy, but mainly at its south and north flanks. There, κ_ρ is elevated by an order of magnitude due to eddy-induced geostrophic shear. Mixing in the eddy core is at the background level with no indication of enhancement.

1. Introduction

The North Pacific low-latitude western boundary current system (LLWBC) entails complex interactions between the Mindanao Current (MC), the Mindanao Eddy (ME), the North Equatorial Current (NEC), and the North Equatorial Counter Current (NECC). It is of crucial importance to the global climate system, as it contributes a large fraction of the subtropical-to-tropical transport of mass, heat, and salt (e.g., Grenier et al., 2011; Lu et al., 1998; Qin et al., 2015), provides the source waters for the Indonesian Throughflow (ITF) (e.g., Gordon & Fine, 1996; Nie et al., 2016), and modulates water mass characteristics of the western Pacific warm pool and the Pacific equatorial current system (e.g., Hu et al., 2015; Lukas et al., 1996).

Because of the confluence of water masses of different origins, the North Pacific LLWBC has been observed to involve substantial water mass transformations and exchanges through mixing both along and across isopcynals (e.g., Fine et al., 1994; Li & Wang, 2012; Lukas et al., 1996). The latter, referred to as diapycnal mixing in the oceanographic literature, is mainly due to small-scale turbulence generated in the ocean interior by the breaking of internal gravity waves or/and instability resulting from the vertical shear of horizontal currents (e.g., Thorpe, 2005). Turbulent mixing is therefore of crucial importance to the dynamics and thermodynamics of the North Pacific LLWBC. Additionally, it impacts on a variety of ocean-atmosphere processes that are of global climate significance, the El Niño–Southern Oscillation (ENSO) being the best known example (e.g., Hu et al., 2015; Moum et al., 2013). However, our knowledge of diapycnal mixing in the North Pacific LLWBC remains quite limited, and consequently, the essential physics responsible for the mixing is missing in current ocean and climate models (e.g., Furue et al., 2015; Richards et al., 2012). In particular, there have been no reports of direct measurements of small-scale turbulence until the present study.

We report here on the first measurements of turbulence microstructure in the North Pacific LLWBC, aiming at a first-order understanding of mixing characteristics in this globally crucial regime. In particular, we test the speculation that diapycnal mixing is elevated in the North Pacific LLWBC (e.g., Li & Wang, 2012; Lukas et al., 1996), which is supported by recent *indirect* estimates of diapycnal diffusivity (κ_ρ) made by applying a semiempirical formula, the so-called fine-scale parameterization of turbulence (e.g., Alberty et al., 2017; Gregg et al., 2003; Polzin et al., 2014), to CTD (conductivity-temperature-depth) and LADCP (lowered acoustic Doppler current profiler) data (Yang et al., 2014). It will be shown that our measurements do *not* support

such a speculation. In fact, diapycnal mixing is found to be very weak in the North Pacific LLWBC, with κ_ρ mostly $O(10^{-6})$ m^2 s^{-1}. Elevated mixing is found to be associated with the ME, a permanent cyclonic eddy. This elevation, however, does not occur through the entire eddy, but mainly at its south and north flanks, where $\kappa_\rho \sim O(10^{-5})$ m^2 s^{-1} appears to be sustained by eddy-induced geostrophic shear. Mixing in the eddy core is at the background level (i.e., $\kappa_\rho \sim O(10^{-6})$ m^2 s^{-1}) with no indication of enhancement.

These results may look surprising in light of the above mentioned speculation but are in fact consistent with predictions from internal wave-wave interaction theory, namely, that mixing induced by the breaking of internal waves is significantly reduced at low latitudes (Henyey et al., 1986; Gregg et al., 2003). The complex interactions among the North Pacific LLWBC and the confluence of different water masses may contribute to the velocity shear for turbulence generation, but that contribution does not seem to be significant except for such prominent dynamic features as the ME. We therefore characterize the North Pacific LLWBC as a weak mixing regime associated with reduced breaking of internal waves at low latitudes.

2. The Data

To study mixing characteristics in the North Pacific LLWBC, we participated in a cruise of the R/V *Kexue* to the tropical western North Pacific Ocean in the summer of 2014. Turbulence microstructure measurements were made along two orthogonal transects in the western boundary region of the tropical North Pacific east of the Philippines on 23 August to 12 September (Figure 1c). The zonal transect was along 8°N from 127.5°E to 135.5°E, and the meridional transect was along 130°E from 1.2°N to 16°N. These were designed to observe turbulent mixing in a broad area of the North Pacific LLWBC, including regions associated with the ME, a permanent cyclonic eddy in the retroflection area of the MC (Figure 1).

There were in total 32 observation sites, with a nominal spacing of 0.5° along each transect. At each site, a series of one to three consecutive casts of the free-fall vertical microstructure profiler (VMP, Rockland Scientific Inc.) were launched to obtain profiling measurements of the temperature, conductivity, and microscale velocity shear from the sea surface down to a depth of up to 600 m. The maximum depth of the casts varied as a result of different weather and oceanographic conditions.

The processing of the microstructure data followed recommendations of Roget et al. (2006) using instrument and probe specifics provided by the manufacturer. The turbulent kinetic energy (TKE) dissipation rate (ε) was calculated by fitting the Nasmyth spectrum to the measured shear spectra over consecutive segments of 2 s. As a result, vertical profiles of ε were obtained with a vertical spacing of $\sim$1.2 m. The same spacing was adopted for profiles of the potential temperature (θ), salinity (S), potential density (σ_θ), and the squared buoyancy frequency (N^2). The profiles of κ_ρ were estimated from profiles of ε and N^2 using the Osborn (1980) formula, $\kappa_\rho = 0.2\varepsilon/N^2$. Here a canonical value 0.2 of the mixing efficiency was adopted, although it has long been understood that the mixing efficiency is unlikely to be constant (e.g., Gregg et al., 2018). Due to contamination by the ship's wake, the turbulence measurements and thus the estimated ε and κ_ρ were unreliable in the top $\sim$10 m. These data were therefore excluded from further analysis.

3. Results

3.1. General Features of Currents and Hydrography

As sketched in Figure 1a, the North Pacific LLWBC originates from the bifurcation of the NEC near the Philippine coast. It mainly consists of the equatorward flowing MC and the permanent cyclonic eddy ME. It contributes to the global overturning circulation through the ITF and closes the interior North Pacific Sverdrup transport via the NECC (e.g., Schönau & Rudnick, 2017). Dynamic variability of the system is therefore essentially determined by the variations of the currents and their interactions. In particular, circulation features and thermohaline structures in the study region are greatly influenced by the ME and its interactions with the neighboring currents (Figures 1b and 1c). During the field sampling period, the eddy-induced currents were stronger on the south and north flanks than in the rest of the ME (Figures 1c and 1a). Currents were also strong at the west end of the zonal transect, where the MC appeared to be intensified by the recirculation associated with the ME (Figures 1c and 4a). As will be shown later, these circulation features had significant impacts on mixing characteristics in the study region.

Running at the crossroads of different water masses, the North Pacific LLWBC is strongly influenced by the thermocline and intermediate waters from higher latitudes. This is most evident in the salinity field (Figure 2b). The upper ocean (depth < 600 m) features a layered distribution of salinity, with saltier thermocline
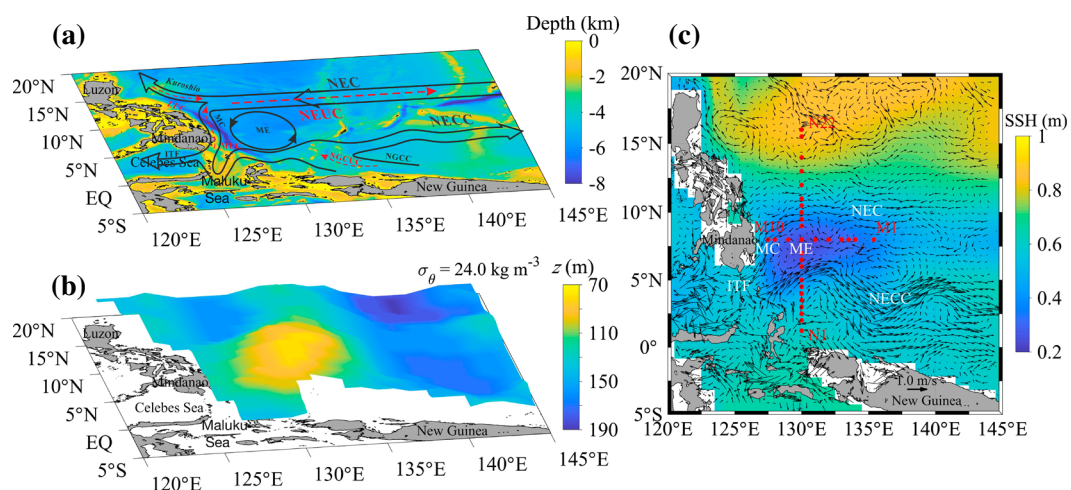
Figure 1. (a) Schematic of major currents in the tropical western Pacific Ocean. NEC, North Equatorial Current; Kuroshio, Kuroshio Current; LUC, Luzon Undercurrent; MC, Mindanao Current; MUC, Mindanao Undercurrent; ME, Mindanao Eddy; NECC, North Equatorial Counter Current; NGCUC, New Guinea Coastal Undercurrent; NGCC, New Guinea Coastal Current; ITF, Indonesian Throughflow. Colors indicate the bathymetry (ETOPO2). (b) Depth of the 24.0 σ_θ isopycnal showing subsurface structure of the Mindanao Eddy (Argo). (c) Map of the tropical western Pacific Ocean showing sites of turbulence microstructure measurements (red bullets) in the background of the sea surface height (colored) and surface geostrophic currents (vectors) during the observation period (Archiving, Validation, and Interpretation of Satellite Oceanographic data). Circulation features relevant to the turbulence measurements are marked.

water situated between fresher surface and intermediate waters. The fresher surface water, with a salinity below 34.4 practical salinity unit (psu), is formed locally due to high precipitation related to the Intertropical Convergence Zone and the upward component of the Walker Cell. The intermediate water masses, which include the North Pacific Intermediate Water (NPIW) and the Antarctic Intermediate Water (AAIW), are also relatively fresher ($S < 34.6$ psu), as they are formed in the subpolar regions where precipitation dominates over evaporation.

There are distinct salinity structures in the thermocline (Figure 2a), that is, there are two salinity maxima spreading southward and northward, respectively (Figure 2b). These are the North Pacific Tropical Water (NPTW) and the South Pacific Tropical Water (SPTW). In the study region, the NPTW has a salinity maximum of 35.2 psu at 23.4 σ_θ, while the SPTW has a salinity maximum of 35.5 psu at 24.9 σ_θ (Figure 2c). Their salinity decreases gradually in the course of spreading as a result of mixing with ambient fresher waters. At the sampled 130°E transect, the water masses seem to converge near 5°N, where the thermocline salinity decreases to a minimum of about 34.8 psu (Figure 2b).

The most intriguing observed dynamic feature is the ME. As evident from Figures 2a and 2b, the isopycnals display a striking dome shape centering around the node of the two sampled transects, that is, 8°N, 130°E. This is consistent with the Argo measurements of subsurface thermohaline structures made during the field sampling period (Figure 1b), as well as the satellite altimetry observations of sea surface height and corresponding surface geostrophic currents (Figure 1c). As designed, the two sampled transects cut across the ME, allowing us to examine the variability of mixing characteristics in relation to the ME and within the large background of the North Pacific LLWBC.

3.2. Turbulent Dissipation in the Surface Mixed Layer

It is typical of the world's open oceans that turbulence is intensified in the surface mixed layer (ML), due to surface wind forcing, wave breaking, and positive surface buoyancy fluxes, even under relatively calm weather conditions. The weather was quite calm (the wind speed at 10 m above the sea surface $W_{10} < 2$ m s^{-1}) during the zonal transect, but it was rough ($W_{10} > 10$ m s^{-1}) for the meridional transect. This is strikingly reflected in the observed turbulent dissipation rate in the ML (Figure 2d). The TKE dissipation rate ε in the ML was up to 10^{-6} W kg^{-1} during the meridional transect, while it was mostly two orders of magnitude lower in the zonal transect.
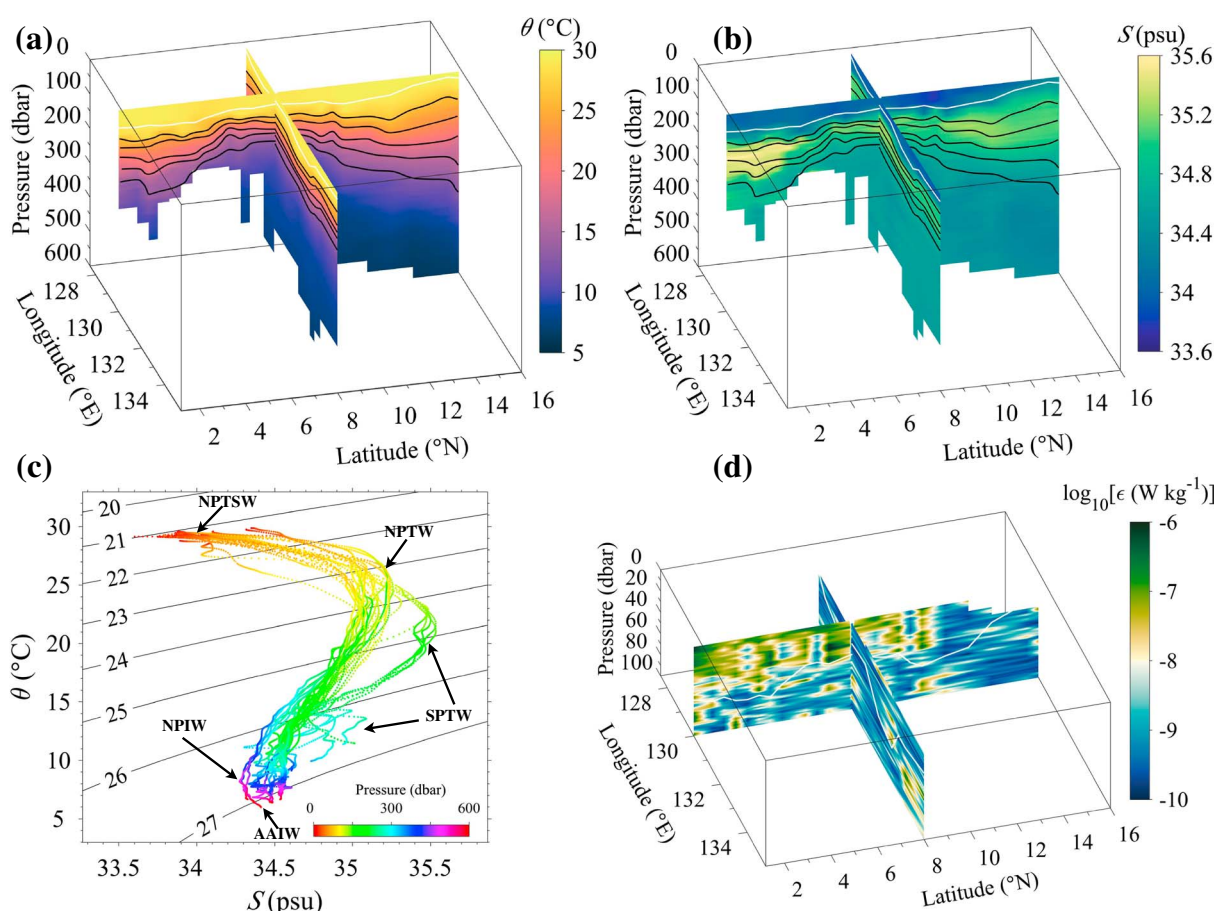
Figure 2. (a, b) Observed potential temperature (θ) and salinity (S) among the two transects. White lines indicate the depth of the ML according to the 0.1 kg m^{-3} density criteria, and contours of the potential density are overlain to indicate variation of the pycnocline (thermocline). (c) The θ-S diagram showing observed water masses with depth (pressure) indicated by colors. NPTSW, North Pacific Tropical Surface Water; NPTW, North Pacific Tropical Water; SPTW, South Pacific Tropical Water; NPIW, North Pacific Intermediate Water; AAIW, Antarctic Intermediate Water. (d) Observed TKE dissipation rate (ε) in the upper 100 m embracing the surface mixed and mixing layers. White lines indicate the depth of the ML.

Note that estimation of the diapycnal diffusivity κ_ρ using the Osborn (1980) formula (with a constant mixing efficiency of 0.2) is problematic in the ML, because in the limit of very weak stratification the efficiency of turbulent mixing is expected to be substantially lower, with most of the TKE dissipated into heat without generating much buoyancy flux. We hereafter focus the analysis on mixing characteristics in the thermocline.

3.3. Weak Thermocline Mixing in the North Pacific LLWBC

In the thermocline, turbulence is suppressed by stable density stratification and is therefore usually substantially weaker than that in the ML. In the study region, the stratification was mainly governed by the vertical gradients of temperature (Figure 2a), with the vertical gradients of salinity making positive and negative contributions, respectively, above and below the salinity maximum (Figure 2b).

The results of turbulent dissipation and mixing estimates below the surface mixed and mixing layers are shown in Figure 3 (for the meridional transect) and Figure 4 (for the zonal transect). To facilitate understanding of the observed turbulence and mixing, flow and stratification properties at the two transects are also shown (Figures 3a–3d and 4a–4d). Without concurrent in situ measurements of the velocity we have resorted to high-resolution data-assimilated numerical modeling results (HYCOM, https://hycom.org) for the estimates of the shear squared (Figures 3b and 4b) and thus the gradient Richardson number (Ri = N^2/S^2 with S^2 being the magnitude of the shear squared; Figures 3d and 4d). For comparison, these were also estimated by considering only the cross-transect component of the geostrophic shear, calculated from the observed density distribution along the transects using the thermal wind relationship (results not shown limited by space).
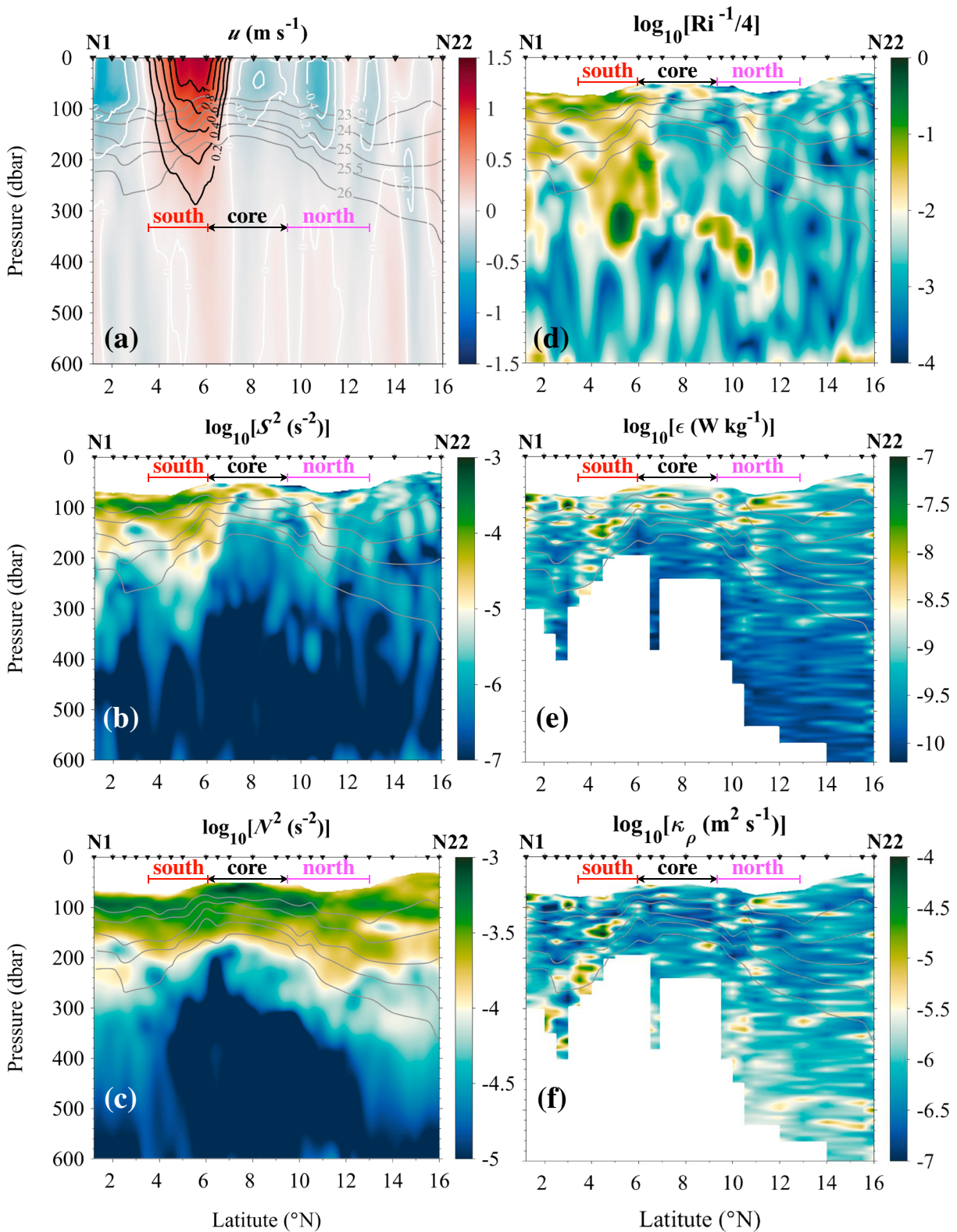
Figure 3. Measured and simulated (HYCOM) variability along the meridional transect. (a–d) Simulated zonal velocity (u), shear squared (S^2), squared buoyancy frequency (N^2), and the inverse gradient Richardson number (Ri^{-1}). (e, f) Observed TKE dissipation rate (ε) and diapycnal diffusivity (κ_ρ) below the surface mixed and mixing layers. Contours of the potential density are overlain to indicate variation of the pycnocline (thermocline). In the plots, the south flank, core region, and north flank of the ME are indicated by "south," "core," and "north," respectively. Locations of the observation sites (N1, · · · , N22) are indicated by inverted triangles.
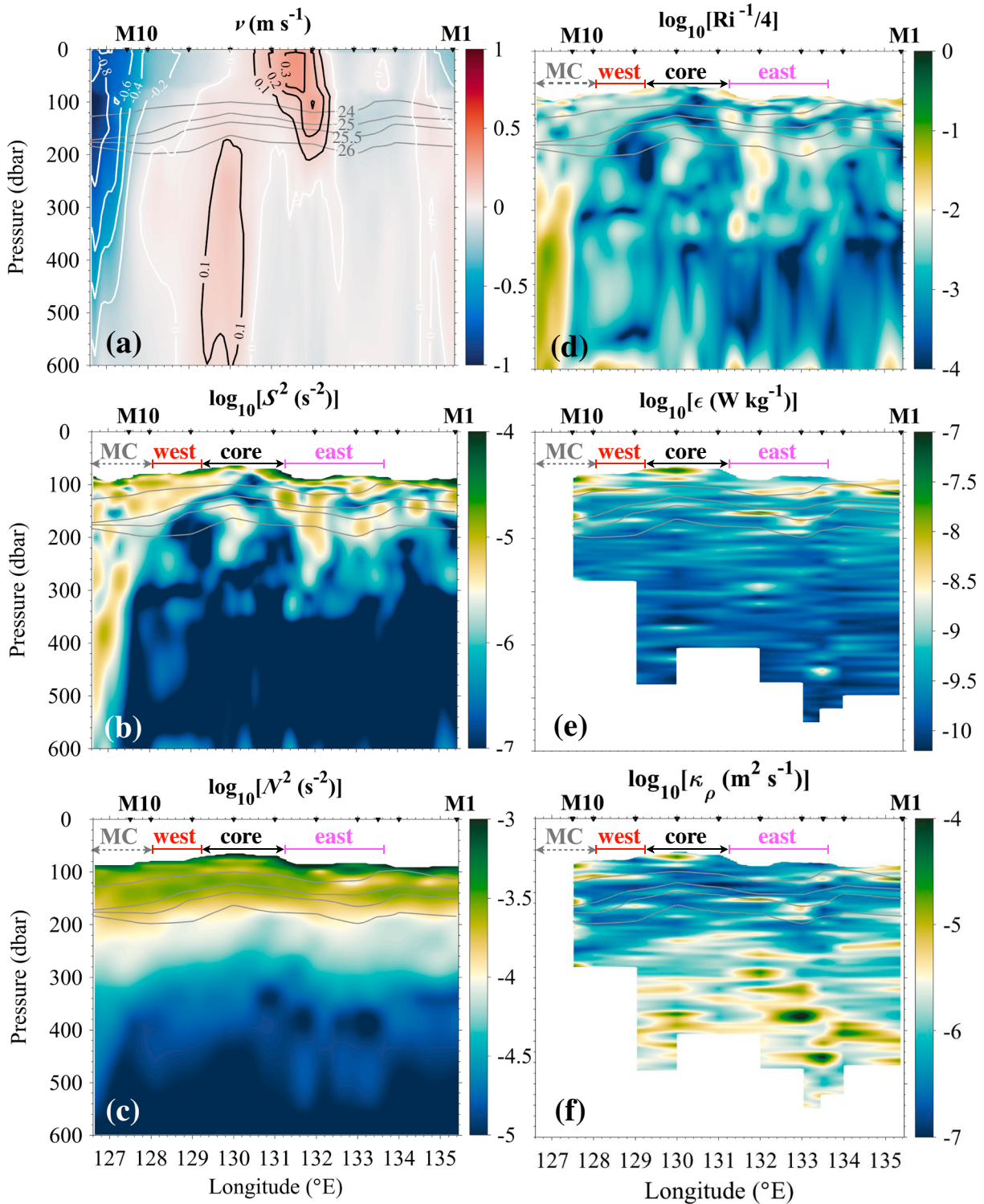
Figure 4. Measured and simulated (HYCOM) variability along the zonal transect. (a–d) Simulated meridional velocity (v), shear squared (S^2), squared buoyancy frequency (N^2), and the inverse gradient Richardson number (Ri^{-1}). (e, f) Observed TKE dissipation rate (ε) and diapycnal diffusivity (κ_ρ) below the surface mixed and mixing layers. Contours of the potential density are overlain to indicate variation of the pycnocline (thermocline). In Figures 4b–4f, the east flank, core region, and west flank of the ME are indicated by "east," "core," and "west," respectively. Locations of the observation sites (M1, · · · , M10) are indicated by inverted triangles.

Neither of the two estimates is robust, as the former depends on the reliability of the simulated flow field while the latter considers only one component of the geostrophic shear. Nevertheless, given that the two estimates reveal very similar spatial structures with regard to the contrast between the core and flanks of the ME (Figures 3d and 4d) and that there is clear correspondence between enhanced turbulence and low Ri (Figures 3d–3f and 4d–4f), we could conclude that the estimated Ri reflects general features of flow stability in the study region and that the model-simulated currents can be referred to in the analysis of the observed turbulence and mixing characteristics. In fact, the simulated and observed density structures agree rather well (Figures 3c and 4c), and the simulated surface currents are almost identical to the satellite altimetry observations (compare Figure 1c with Figures 3a and 4a; this is not surprising though, as altimetry data were assimilated in the numerical simulations). Note, however, that fluctuations in Ri due to the breaking of internal waves cannot be resolved by either of the two estimates.

It is evident from Figures 3e–3f and 4e–4f that turbulent dissipation and mixing are overall very weak in the thermocline. The TKE dissipation rate ε was mostly of $O(10^{-10})$ W kg^{-1}, and the diapycnal diffusivity κ_ρ was mostly of $O(10^{-6})$ m^2 s^{-1}, which are at the lower ends of thermocline turbulence and mixing in the world's oceans (Thorpe, 2005; Waterhouse et al., 2014). This is contrary to the prevailing speculation that diapycnal mixing may be elevated in the North Pacific LLWBC (e.g., Lukas et al., 1996; Li & Wang, 2012; Yang et al., 2014). Note, however, that the results are consistent with predictions from internal wave-wave interaction theory, namely, that mixing induced by the breaking of internal waves is significantly reduced at low latitudes (Henyey et al., 1986; Gregg et al., 2003). It is thus suggested that, although the interactions of currents in the North Pacific LLWBC and the confluence of different water masses may contribute to the velocity shear for turbulence generation, that contribution does not seem to be significant. Instead, thermocline turbulence appears to be essentially sustained by the breaking of internal waves, which as predicted by the theory is rather weak. The North Pacific LLWBC is therefore a weak mixing regime of the world's oceans.

The suppression of turbulence in the thermocline is also reflected in the distribution of Ri, which is color coded in terms of $\log_{10}(\text{Ri}^{-1}/4)$ in Figures 3d and 4d to highlight regions with Ri between 0.25 and 25 (i.e., $\log_{10}(\text{Ri}^{-1}/4)$ between 0 and −2). Here 0.25 is a critical value of Ri for shear instability (Thorpe, 2005). One can see that Ri was mostly much larger than 0.25 in the thermocline, usually by at least two orders of magnitude. It decreased dramatically at the flanks of the ME, particularly at its south flank, due to strong eddy-induced velocity shear (Figures 3b and 4b). There seemed to be a trend that both ε and κ_ρ varied inversely with Ri (Figures 3d–3f and 4d–4df).

To gain a quantitative understanding of the statistical characteristics of turbulent dissipation and mixing in the North Pacific LLWBC, we calculated the mean TKE dissipation rate ($<\varepsilon>$) and diapycnal diffusivity ($<\kappa_\rho>$) in the thermocline from the dissipation and mixing estimates. Because we seek to reveal the averaged (background) thermocline mixing characteristics in the region, rather than localized mixing associated with certain dynamic features, we have excluded data from regions apparently influenced by the ME or MC. Mixing characteristics in these regions will be analyzed in the following section. It is found that $<\varepsilon>$ was 4.4×10^{-10} W kg^{-1} with the 95% bootstrapped confidence interval (CI) being $(4.2-4.6) \times 10^{-10}$ W kg^{-1}, and $<\kappa_\rho>$ was 0.83×10^{-6} m^2 s^{-1} (95% CI $(0.80-0.88) \times 10^{-6}$ m^2 s^{-1}). This is consistent with our visual observations from Figures 3e–3f and 4e–4f, confirming that the study region is a weak mixing regime.

3.4. Mixing Variability in the Mindanao Eddy

We have shown that thermocline turbulence and mixing are overall very weak in the North Pacific LLWBC. It is, however, rather striking from Figures 3e–3f and 4e–4f that there was enhanced turbulence at the flanks of the ME. This is most evident in the meridional transect (Figures 3e and 3f), where the dome structure of the isopycnals was very pronounced, and the eddy-induced currents and shear were very strong at the south and north flanks of the ME (Figures 3a and 3b). Thermocline turbulence was most intensified at the south flank. There, the mean TKE dissipation rate $<\varepsilon>$ was 3.0×10^{-8} W kg^{-1} (95% CI $(2.1-5.5) \times 10^{-8}$ W kg^{-1}), and the mean diapycnal diffusivity $<\kappa_\rho>$ was 2.9×10^{-5} m^2 s^{-1} (95% CI $(2.2-3.8) \times 10^{-5}$ m^2 s^{-1}). At the north flank, both ε and κ_ρ were substantially lower, with $<\varepsilon>$ being 4.2×10^{-9} W kg^{-1} (95% CI $(3.5-5.2) \times 10^{-9}$ W kg^{-1}) and $<\kappa_\rho>$ being 5.9×10^{-6} m^2 s^{-1} (95% CI $(4.8-8.2) \times 10^{-6}$ m^2 s^{-1}). This drastic contrast between the south and north flanks was also reflected in the distribution of Ri (Figure 3d). It was mostly below 25 (i.e., $\log_{10}(\text{Ri}^{-1}/4) > -2$) and often below 2.5 (i.e., $\log_{10}(\text{Ri}^{-1}/4) > -1$) at the south flank, but it was mostly above 25 (i.e., $\log_{10}(\text{Ri}^{-1}/4) < -2$) at the north flank.

At the zonal transect, the impact of the ME seemed substantially weaker with isopycnals being relatively flat, but the eddy-induced geostrophic currents and shear remained significant (Figures 4a and 4b). Thermocline dissipation and mixing appeared to be elevated at the east and west flanks of the ME (Figures 4e and 4f), although much less pronounced than at the south and north flanks (Figures 3e and 3f). At the east flank, the mean TKE dissipation rate $< \varepsilon >$ was 2.0×10^{-9} W kg^{-1} (95% CI $(1.6-2.6) \times 10^{-9}$ W kg^{-1}), and the mean diapycnal diffusivity $< \kappa_\rho >$ was 1.4×10^{-6} m^2 s^{-1} (95% CI $(1.1-1.7) \times 10^{-6}$ m^2 s^{-1}). At the west flank, $< \varepsilon >$ was 2.9×10^{-9} W kg^{-1} (95% CI $(2.3-3.8) \times 10^{-9}$ W kg^{-1}) and $< \kappa_\rho >$ was 2.4×10^{-6} m^2 s^{-1} (95% CI $(2.0-3.1) \times 10^{-6}$ m^2 s^{-1}). Toward the Philippine coast, the impact of the MC appears to become significant. This is evident in the observed thermocline dissipation and mixing. As shown in Figures 4e and 4f, both ε and κ_ρ increased toward the west end of the zonal transect. Closer to the coast, the enhanced shear induced by the MC extended down to a depth of ∼600 m (Figure 4b), where turbulent dissipation and mixing are expected to be substantially elevated. Profiling measurements of turbulence microstructure extending to the Philippine coast are obviously crucial to revealing mixing characteristics in the MC but were unfortunately impossible during this cruise for political reasons.

As shown in Figures 3e–3f and 4e–4f, there is no indication that thermocline turbulence and mixing in the core of the ME were enhanced. This is consistent with the *Ri* distribution (Figures 3d and 4d), whose values were mostly above 25 (i.e., $\log_{10}(Ri^{-1}/4) < -2$) throughout the eddy core. In fact, thermocline dissipation and mixing in the eddy core were similar to that in the large background of the North Pacific LLWBC. The mean TKE dissipation rate in the thermocline was 2.7×10^{-10} W kg^{-1} (95% CI $(2.5-3.0) \times 10^{-10}$ W kg^{-1}), and the mean diapycnal diffusivity in the thermocline was 0.91×10^{-6} m^2 s^{-1} (95% CI $(0.82-1.0) \times 10^{-6}$ m^2 s^{-1}).

4. Discussion

4.1. Comparison With the Fine-Scale Parameterization

We have characterized the North Pacific LLWBC as a weak mixing regime with $\kappa_\rho \sim O(10^{-6})$ m^2 s^{-1}. This is, however, in contrary to the results of Yang et al. (2014) who, based on estimates of κ_ρ from a fine-scale parameterization, suggested that this region is a strong mixing regime with κ_ρ at least two orders of magnitude larger than our estimates (see their Figure 8a). To understand this discrepancy, we made comparisons between microstructure measurements and fine-scale estimates for the thermocline-averaged diapycnal diffusivity ($< \kappa_\rho >_{therm}$) at all our observation sites. We used the strain-based fine-scale parameterization detailed in Kunze et al. (2006). At each site, we first calculated the fine structure-based $< \kappa_\rho >_{therm}$ for each 128-point (∼150 m) segment. Microstructure measurements in the same depth range were then averaged to get the microstructure-based $< \kappa_\rho >_{therm}$.

The comparisons are shown in Figure 5a. Although at some sites the agreement between the two estimates is within a factor of 2, $< \kappa_\rho >_{therm}$ is generally overestimated by the fine-scale parameterization. The overestimation is mostly within a factor of 10 but can also be by up to two orders of magnitude. Note, however, that taking $< \kappa_\rho >_{therm}$ at each site as an independent sample without any averaging, the fine structure-based estimates may suffer rather large uncertainties (Whalen et al., 2015). This may be responsible for some of the discrepancies in the comparisons, but the overestimation seems to be a robust feature. It is thus indicated that the oft-used fine-scale parameterization may be invalid for this LLWBC, although reasonable agreement between microstructure measurements and fine-scale estimates has previously been found both near the equator (Whalen et al., 2015) and in the western boundary currents (Winkel et al., 2002). In fact, the assumptions underlying the fine-scale parameterization are violated near the equator (Gregg et al., 2003; Whalen et al., 2015), and in swift western boundary currents the fine-scale shear and strain variance may be largely due to non-internal wave processes. Therefore, caution should be used when using the fine-scale parameterization for these regions. As such, the contrary results on thermocline mixing in the North Pacific LLWBC seem to suggest that κ_ρ was largely overestimated by Yang et al. (2014), although temporal variability may be responsible for part of the discrepancy.

4.2. Scaling of Thermocline Mixing

Our observations tend to suggest that the weak background mixing in the North Pacific LLWBC is sustained by reduced breaking of internal waves at low latitudes. This mixing may be locally elevated due to strong shear associated with prominent dynamic features such as the ME. As already mentioned, clear correspondence between enhanced turbulence and low Ri can be seen in the observations (Figures 3d–3f and 4d–3f). We thus
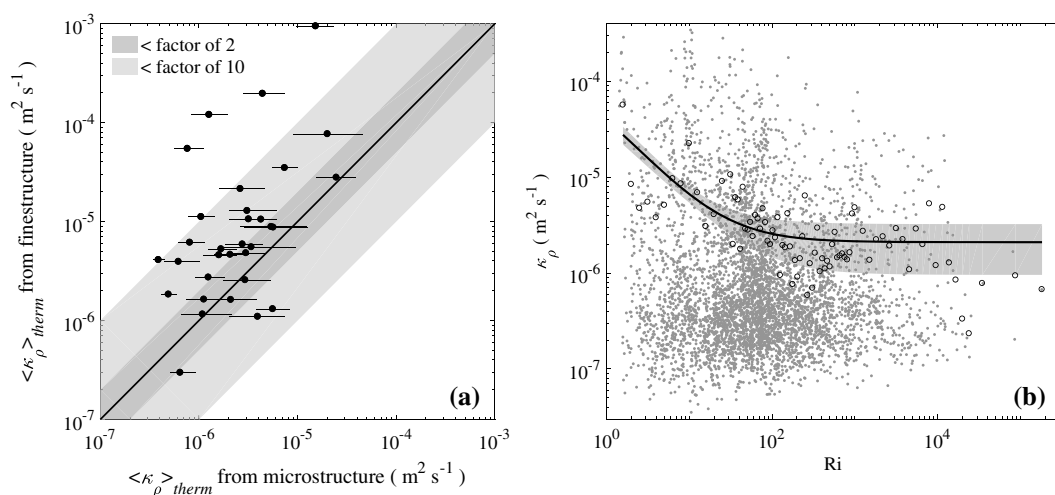
Figure 5. (a) Comparison between microstructure measurements and fine-scale parameterization for the thermocline-averaged diapycnal diffusivity ($<\kappa_\rho>_{therm}$) at all the observation sites. Agreement within factors of 2 and 10 is designated by the gray bands. The 95% bootstrapped confidence intervals for the estimates from microstructure measurements are represented by bars. (b) Original (gray small symbols) and bin-averaged samples (large open symbols) of the diapycnal diffusivity (κ_ρ) versus the gradient Richardson number (Ri) for all the estimates in the thermocline. The bold line shows the analytical approximation discussed in the text with the 95% confidence intervals indicated by gray shading.

seek to model the observed κ_ρ with a background diffusivity (κ_0) and Ri according to the following formula constructed in the general spirit of Munk and Anderson (1948),

$$\kappa_\rho = \kappa_0 + \kappa_m(1 + Ri/Ri_c)^{-1}, \qquad (1)$$

where $Ri_c = 0.25$ is the critical value of Ri for shear instability and κ_m the (maximum) diffusivity corresponding to vanishing Ri. Both κ_0 and κ_m are to be determined from the data. As shown in Figure 5b, although the original data are scattered, the bin-averaged data show a clear decreasing tendency of κ_ρ with increasing Ri. A nonlinear least squares regression of the bin-averaged data using the MATLAB function *nlinfit* gave $\kappa_0 = 2.1 \times 10^{-6}$ m² s⁻¹ and $\kappa_m = 1.9 \times 10^{-4}$ m² s⁻¹. The 95% confidence intervals for the model predictions were also obtained using the MATLAB function *nlpredci* and are shown in Figure 5b as gray shading. One can see that most of the bin-averaged data fall within the confidence intervals, indicating that the analytical model (1) approximates the observations well. Note also that the estimated value of κ_0 is close to the background diffusivity calculated from the data. The success of this simple scaling is encouraging, as κ_ρ is only a function of the model-simulated Ri. This means that the scaling can be easily adopted into regional ocean and climate models of the North Pacific LLWBC.

5. Conclusions

We have reported on the first turbulence microstructure measurements in the North Pacific LLWBC. Thermocline turbulence and mixing were found to be overall very weak, with the TKE dissipation rate $\varepsilon \sim O(10^{-10})$ W kg⁻¹ and the diapycnal diffusivity $\kappa_\rho \sim O(10^{-6})$ m² s⁻¹. Both values are at the low ends of the observed ranges. Elevated mixing with κ_ρ an order of magnitude larger was found at the south and north flanks of the Mindanao Eddy, where mixing enhancement appeared to be due to eddy-induced geostrophic shear.

The results reported here are based on measurements from a single cruise and are therefore by no means definitive. There may be significant temporal variations of thermocline mixing, in particular due to the modulation by ENSO events (Richards et al., 2012). Multiple-cruise observations covering different seasons and various phases of the ENSO cycle would reveal these features.

References

Alberty, M. S., Sprintall, J., MacKinnon, J., Ganachaud, A., Cravatte, S., Eldin, G., … Melet, A. (2017). Spatial patterns of mixing in the Solomon Sea. *Journal of Geophysical Research: Oceans*, *122*, 4021–4039. https://doi.org/10.1002/2016JC012666

Fine, R. A., Lukas, R., Bingham, F. M., Warner, M. J., & Gammon, R. H. (1994). The western equatorial Pacific: A water mass crossroads. *Journal of Geophysical Research*, *99*(C12), 25,063–25,080.

Furue, R., Jia, Y. L., McCreary, J. P., Schneider, N., Richards, K. J., Muller, P., & Kohl, A. (2015). Impacts of regional mixing on the temperature structure of the equatorial Pacific Ocean. Part 1: Vertically uniform vertical diffusion. *Ocean Modelling*, *91*, 91–111.

Gordon, A. L., & Fine, R. A. (1996). Pathways of water between the Pacific and Indian oceans in the Indonesian seas. *Nature*, *379*, 146–149. https://doi.org/10.1038/379146a0

Gregg, M. C., D'Asaro, E. A., Riley, J. J., & Kunze, E (2018). Mixing efficiency in the ocean. *Annual Review of Marine Science*. https://doi.org/10.1146/annurev-marine-121916-063643

Gregg, M. C., Sanford, T. B., & Winkel, D. P. (2003). Reduced mixing from the breaking of internal waves in equatorial waters. *Nature*, *422*, 513–515. https://doi.org/10.1038/nature01507

Grenier, M., Cravatte, S., Blanke, B., Menkes, C., Koch-Larrouy, A., Durand, F., … Jeandel, C. (2011). From the western boundary currents to the Pacific Equatorial Undercurrent: Modeled pathways and water mass evolutions. *Journal of Geophysical Research*, *116*, C12044. https://doi.org/10.1029/2011JC007477

Henyey, F. S., Wright, J., & Flatte, S. M. (1986). Energy and action flow through the internal wave field: An eikonal approach. *Journal of Geophysical Research*, *91*, 8487–8495.

Hu, D., Wu, L., Cai, W., Sen Gupta, A., Ganachaud, A., Qiu, B., … Kessler, W. S. (2015). Pacific western boundary currents and their roles in climate. *Nature*, *522*, 299–308. https://doi.org/10.1038/nature14504

Kunze, E., Firing, E., Hummon, J. M., Chereskin, T. K., & Thurnherr, A. M. (2006). Global abyssal mixing inferred from lowered ADCP shear and CTD strain profiles. *Journal of Physical Oceanography*, *36*(8), 1553–1576. https://doi.org/10.1175/JPO2926.1

Li, Y., & Wang, F. (2012). Spreading and salinity change of North Pacific tropical water in the Philippine Sea. *Journal of Oceanography*, *68*, 439–452. https://doi.org/10.1007/s10872-012-0110-3

Lu, P., McCreary Jr., J. P., & Klinger, B. A. (1998). Meridional circulation cells and the source waters of the Pacific Equatorial Undercurrent. *Journal of Physical Oceanography*, *28*(1), 62–84.

Lukas, R., Yamagata, T., & McCreary, J. P. (1996). Pacific low-latitude western boundary currents and the Indonesian Throughflow. *Journal of Geophysical Research*, *101*(C5), 12,209–12,216.

Moum, J. N., Perlin, A., Nash, J. D., & McPhaden, M. J. (2013). Seasonal sea surface cooling in the equatorial Pacific cold tongue controlled by ocean mixing. *Nature*, *500*, 64–67. https://doi.org/10.1038/nature12363

Munk, W. H., & Anderson, E. R. (1948). Notes on the theory of the thermocline. *Journal of Marine Research*, *3*, 276–295.

Nie, X., Gao, S., Wang, F., & Qu, T. (2016). Subduction of North Pacific Tropical Water and its equatorward pathways as shown by a simulated passive tracer. *Journal of Geophysical Research: Oceans*, *121*, 8770–8786. https://doi.org/10.1002/2016JC012305

Osborn, T. R. (1980). Estimates of the local rate of vertical diffusion from dissipation measurements. *Journal of Physical Oceanography*, *10*, 83–89.

Polzin, K. L., Naveira Garabato, A. C., Huussen, T. N., Sloyan, B. M., & Waterman, S. (2014). Finescale parameterizations of turbulent dissipation. *Journal of Geophysical Research: Oceans*, *119*, 1383–1419. https://doi.org/10.1002/2013JC008979

Qin, X., Sen Gupta, A., & van Sebille, E. (2015). Variability in the origins and pathways of Pacific Equatorial Undercurrent water. *Journal of Geophysical Research: Oceans*, *120*, 3113–3128. https://doi.org/10.1002/2014JC010549

Richards, K. J., Kashino, Y., Natarov, A., & Firing, E. (2012). Mixing in the western equatorial Pacific and its modulation by ENSO. *Geophysical Research Letters*, *39*, L02604. https://doi.org/10.1029/2011GL050439

Roget, E., Lozovatsky, I., Sanchez, X., & Figueroa, M. (2006). Microstructure measurements in natural waters: Methodology and applications. *Progress in Oceanography*, *70*(2–4), 126–148.

Schönau, M., & Rudnick, D. (2017). Mindanao current and undercurrent: Thermohaline structure and transport from repeat glider observations. *Journal of Physical Oceanography*, *47*(8), 2055–2075.

Thorpe, S. A. (2005). *The turbulent ocean* (pp. 485). Cambridge: Cambridge University Press.

Waterhouse, A. F., MacKinnon, J. A., Nash, J. D., Alford, M. H., Kunze, E., Simmons, H. L., … Craig, M. (2014). Global patterns of diapycnal mixing from measurements of the turbulent dissipation rate. *Journal of Physical Oceanography*, *44*(7), 1854–1872.

Whalen, C. B., MacKinnon, J. A., Talley, L. D., & Waterhouse, A. F. (2015). Estimating the mean diapycnal mixing using a finescale strain parameterization. *Journal of Physical Oceanography*, *45*(4), 1174–1188. https://doi.org/10.1175/JPO-D-14-0167.1

Winkel, D. P., Gregg, M. C., & Sanford, T. B. (2002). Patterns of shear and turbulence across the Florida Current. *Journal of Physical Oceanography*, *32*(11), 3269–3285.

Yang, Q., Zhao, W., Li, M., & Tian, J. (2014). Spatial structure of turbulent mixing in the northwestern Pacific Ocean. *Journal of Physical Oceanography*, *44*(8), 2235–2247.